Analyst

Production of Mixed Element Actinide Reference Particulates to Support Nuclear Safeguards using THESEUS, an Aerosol-based Particulate Synthetic Methodology

Journal:	*Analyst*
Manuscript ID	AN-ART-10-2022-001774.R2
Article Type:	Paper
Date Submitted by the Author:	08-May-2023

Complete List of Authors:	Naes, Benjamin ; Los Alamos National Laboratory Scott, Spencer; Savannah River National Laboratory Waldron, Abigail; Savannah River National Laboratory, Lawson, Seth; Savannah River National Laboratory Bronikowski, Michael; Savannah River National Laboratory Gleaton, Laken; Savannah River National Laboratory Smith, Ross; Savannah River National Laboratory Wurth, Kimberly; Los Alamos National Laboratory Tenner, Travis; Los Alamos National Laboratory Wellons, Matthew; Savannah River National Laboratory

ARTICLE

Production of Mixed Element Actinide Reference Particulates to Support Nuclear Safeguards using THESEUS, an Aerosol-based Particulate Synthetic Methodology

Received 00th January 20xx,
Accepted 00th January 20xx

DOI: 10.1039/x0xx00000x

SRNL-STI-2022-00568

Benjamin E. Naes,[a] Spencer Scott,[b] Abigail Waldron,[b] Seth Lawson,[b] Michael G. Bronikowski,[b] Laken I. Gleaton,[b] Ross J. Smith,[b] Kimberly N. Wurth,[a] Travis J. Tenner[a] and Matthew Wellons*[b]

The THermally Evaporated Spray for Engineered Uniform particulateS (THESEUS) production platform was developed to generate highly uniform mixed actinide oxide particles. The particulate synthesis platform builds on previous efforts and utilizes an aerosol-based technology to generate, calcine, characterize, and aggregate a monodisperse oxide phase particle product. In this study, particles comprised of uranium oxide, incorporated with varying compositions of thorium, were produced. Th/U test materials with ^{232}Th concentrations between 1 ppm and 10%, ratioed to ^{238}U, were successfully generated with in situ calcination at 600 °C and characterized by in situ aerodynamic particle size spectrometry and ex situ microanalytical methods. Populations of monodisperse particulates (geometric standard deviation - GSD < 1.15) with an average diameter near 1-µm were generatated and micro-Raman spectroscopy of individual particles identified U_3O_8 as the primary material phase for the range of Th/U samples analyzed. Single particle measurements and automated particle analyses by secondary ion mass spectrometry (SIMS) were performed. Uniform inter-particle elemental and isotopic homogeneity for uranium and thorium isotopes was characterized by SIMS, and a ^{232}Th/^{238}U relative sensitivity factor of 0.53 was determined. SIMS results demonstrated differences in the ^{232}Th/^{238}U profiling behavior for Th/U particulates with increased Th content (> 1 %). Despite the observed profiling behavior, single particle measurements of the 10% Th sample indicate inter-particle homogeneity. This work represents the first systematic study of Th/U microparticulate reference materials generated and intended for nuclear safeguards applications and serves as a demonstration of THESEUS to support a sustained capability for the production mixed-element particulate reference materials.

1. Introduction

The detection of undeclared nuclear activities under international safeguards is a key activity performed by the International Atomic Energy Agency's (IAEA) Environmental Sample Laboratory (ESL). In part, nuclear safeguards verification includes the collection of environmental samples within declared or decommissioned facilities, shipment of those samples back to ESL in Vienna, Austria, and distribution of collected samples to a Network of Analytical Laboratories (NWAL) for bulk and particle analysis.[1] The characterization of particulate-based samples within these environmental swipe samples plays a critical role in the IAEA's ability to assure the absence of undeclared nuclear activities. IAEA and NWAL quality assurance and quality control (QA/QC) operations require fit-for-purpose reference particulates with tailored and uniform isotopic and elemental compositions, in addition to uniform particulate size, morphology, and material phase.[2-4] However, actinide reference micro-particulates are not readily available, which limits the overall analytical approach. Production of mixed actinide-bearing particulate materials are therefore in demand and necessary to address a variety of current nuclear safeguards analytical challenges.[5]

To assist IAEA nuclear safeguards operations, multiple Member State Support Programs (MSSP) in support of the IAEA have conducted, and continue to conduct, a variety of parallel complimentary R&D and manufacturing programs.[6] The development efforts have sought to mature and operationalize relevant synthesis methods for actinide-bearing particulates for QC purposes. The technologies pursued thus far can be divided into two categories: hydrothermal chemical synthesis[7-10] and aerosol-based spray drying.[4, 11, 12] Both methodologies have demonstrated viability for the manufacture of uranium oxide, fit-for-purpose QC materials, with varying and targeted ^{235}U/^{238}U isotopic compositions. The desired specifications of the engineered particulate materials have focused on various analytical use aspects, including particle size (i.e., mean value) and population distribution targets, specifically particulates 1 µm in diameter and monodisperse populations. Other important considerations or specifications may include, but are not limited to, particulate impurities, shelf-life stability, material phase (e.g., UO_2 and U_3O_8) and physical form. Engineering developmental efforts for uranium-bearing QC reference particulates continue and include: (1) scaling up the manufacturing processes, (2) developing a pedigree of

[a] Los Alamos National Laboratory, New Mexico, USA.
[b] Savannah River National Laboratory, South Carolina, USA. Email: Matthew.Wellons@srnl.doe.gov

commercially available particulate laden substrates, and (3) shelf-life characterization studies.[3, 11-13]

Production of mixed actinide test particulates with tailored elemental and isotopic compositions of uranium, thorium, and/or plutonium continues to be challenging. This is due to the need for precise elemental and isotopic ratios, while maintaining a high-degree of interparticle homogeneity. Complicating factors which may adversely impact the quality of the generated test materials include: the potential for cross-contamination between batches of material, i.e., a memory effect within the production system, the potential for environmental contamination with particulates of undesirable elemental or isotopic composition, and the potential for elemental or isotopic fractionation prior to, or during, the particle formation process. Efforts to produce actinide-bearing test particulates stems back to early production efforts in the 1990s.[14, 15] Current analytical material needs include uranium oxide particulates with added lanthanides, metals, and/or other trace constituents. These mixed element QC test materials are invaluable for characterizing environmental samples derived from nuclear reactors and reprocessing facilities. In addition, such materials are imperative to advance microanalytical capabilities, such as particle-based chronometry.[16-19] Recent R&D efforts have focused on transitioning uranium oxide production technologies to the synthesis of mixed actinide-bearing particulates with targeted lanthanide compositions[20-22], and Th/U-oxide particles.[23] Savannah River National Laboratory (SRNL) has developed a mixed actinide oxide phase particle production platform to meet end user physical and analytical requirements. Prior, SRNL has explored various particulate synthesis parameters, such as calcination temperature, feedstock concentration, ratios of feedstock solutions, and aerosol generation, which improved production.[5-7,16, 17]

The engineered aerosol-based production platform developed is called THESEUS, which stands for THermally Evaporated Spray for Engineered Uniform particulateS. This methodology is used to produce fit-for-purpose mixed-actinide particulate species, suitable for QC reference materials. For this study, generated uranium oxide particulates were varied compositionally by the addition of thorium. Particulates containing no added Th to samples with 10% (mol) Th ratioed to ^{238}U were produced and analyzed. The particles display equivalent circular diameters (ECD) near 1-µm, while maintaining a monomodal distribution with geometric standard deviations (GSD) less than or equal to 1.15. Characterization included large geometry secondary ion mass spectrometry (LG-SIMS) and was utilized to measure the extent of interparticle isotopic and elemental homogeneity. Additional efforts included scanning electron microscopy (SEM) and aerodynamic-based measurements were used to assess particle size and morphological uniformity.

2. Experimental Procedure

2.1 Particle Generation Platform

Uranium-thorium particles were generated with an aerosol-based approach, with modifications to a previously developed production platform.[12] The particle production platform consists of the following components: a Flow Focusing Monodisperse Aerosol Generator (FMAG, Model 1520, TSI Inc), for droplet generation, a diffusion drier (Model 3062, TSI Inc.) and an Aerodynamic Particle Sizer (APS, Model 3321, TSI Inc.),

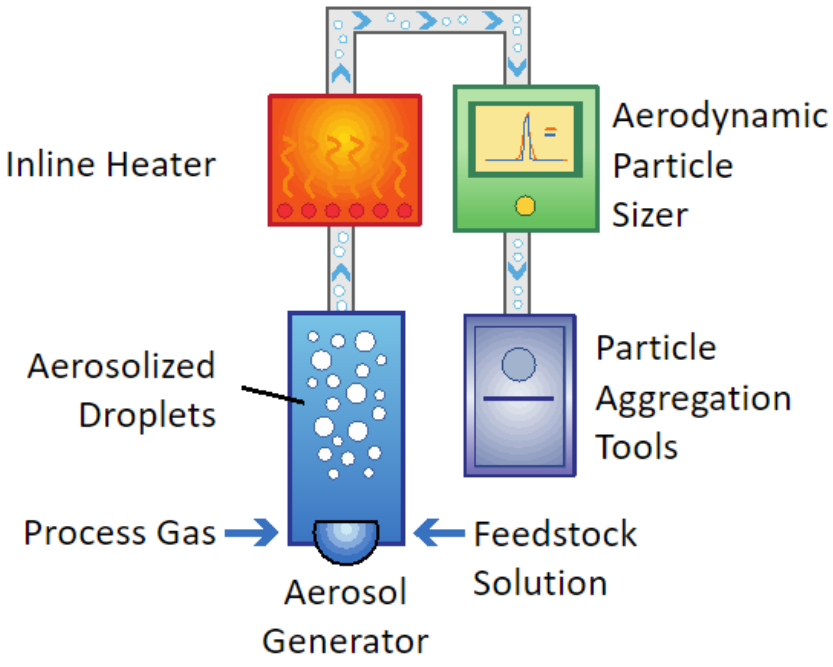

Figure 1 Diagram of the THermally Evaporated Spray for Engineered Uniform particulateS (THESEUS) production platform used in this work. Aerosol flow direction originates from the Generator and terminates within the collector housed in the Radioactive Containment

to provide in situ particle size information. Additionally, THESEUS is equipped with an inline heater (Heat Torch 050, Tutco-Farnam Inc.), a HEPA exhaust filter, and a variant of an Aerosol Contaminant Extractor (ACE), an SRNL-designed electrostatic precipitator for aerosolized particle collection.[24-26] Electrostatic precipitation enabled the collection of particulates on silicon and carbon substrates without the use of additional working media, such as mineral oil, grease, or adhesives, which may deleteriously impact the analysis of the particles. The process gas used for particle generation was compressed air. The platform was entirely assembled and operated within a radiological chemical hood per standard safety guidelines. This modified version of the production platform, THESEUS, is shown schematically in Figure 1.

One notable design change to the THESEUS platform, versus previous particle production campaigns[21], is the inclusion of the inline heater, mentioned above, which enabled the thermal conversion of the aerosolized particles to a more stable oxide phase at temperatures up to 600 °C. Modifications were also made to the particle flight path, to ensure adequate cooling prior to collection. Also, the new version of the production platform includes the ability to perform aerodynamic particle size measurements prior to and after passing through the inline heater, which enables the investigation of heating effects on both aerodynamic properties of the particles, as well as an assessment of distributional effects within the particle population as they pass through the heater. The platform is completely configurable with manual valves per given experimental design requirements. Note that the generated aerosol stream can be characterized via the inline APS, with or without passing through the diffusion dryer and inline heater. In similar fashion the aerosol stream can be directed either to a waste HEPA filter or transferred into the radioactive containment enclosure for collection. For this effort, no attempt was made to remediate potential cross-contamination of particulates between production batches with differing Th/U feedstock concentrations.

The feedstock solutions used in particle production were prepared using uranyl oxalate and thorium nitrate dissolved in ultrapure water. The uranyl oxalate was prepared from legacy (depleted) uranium at SRNL with 0.17% ^{235}U isotope composition, and the thorium nitrate was prepared from legacy (natural) thorium materials at SRNL.[27, 28] Uranyl oxalate and thorium nitrate solutions were prepared by use of calibrated analytical balances and pipets, with nominal measurement errors of ± 0.05 mg and ± 0.001 mL, respectively. Concentrations of 0.84 mg/mL for the combined uranyl oxalate, thorium nitrate solutions were used to generate the nominal 1 µm equivalent circular diameter (ECD) oxide particulates. A target Th/U ratio was formulated using the thorium to uranium feedstock ratios. Preparation of the feedstock solution was performed prior to use in order to mitigate potential chemical reactions in solution. Typical FMAG parameters used in particle production operation included a dilution air flow rate of 15.0 ± 0.1 L/min, a flow focusing air pressure of 2.00 ± 0.05 psi (3.79 ± 0.34 kPa), a feedstock solution injection rate of 3.00 mL/h, and an orifice vibration frequency of 130 kHz, to generate liquid droplets with a diameter near 23 µm. The aerosolized droplets were then heated to 600 °C in-flight and measured using the APS to ensure the desired particle size and verify stable size distributions. Following APS, the flow was re-directed, and particle collection culminated on 1-inch carbon and silicon wafers using an electrostatic precipitator collector.

2.2 Characterization

The generated particulates were characterized using a combination of aerosol and micro-analytical methods. Analytical methods included scanning electron microscopy (SEM), secondary ion mass spectrometry (SIMS), Raman spectroscopy, and aerodynamic particle size spectrometry. The key metrics for characterization included:

1. Mean particle size, calculated as equivalent circular diameter (ECD),
2. Monodispersity evaluation, calculated as geometric standard deviation (GSD),
3. Qualitative assessment of particulate morphologies,
4. Particulate material phase and density, and
5. Uranium and thorium isotopic intra- and inter-particle homogeneity.

In-situ aerodynamic particle size measurements, obtained by Aerodynamic Particle Sizer (APS) were utilized to assess the average particle size of the generated particles, as well as the monodispersity of the generated particles, evaluated by GSD. Specifically, a GSD (σ_G) cuttoff of 1.15 was used in the determination of monodispersity, with the GSD of particle populations equal or less than 1.15 identified as monodisperse, and above 1.15 identified as polydisperse. APS measurements utilized an acquisition time of 20 seconds, resulting in approximately 20,000 particles per measurement. The APS provided 52 size bins in the 0.5 to 20 micron range, with an average APS bin-size in the 0.5 to 2-micron region were 0.077 µm for ρ = 1 g/cm^3, and 0.027 µm for ρ = 8.3 g/cm^3.

High-resolution scanning electron microscopy (SEM) with energy dispersive spectroscopy (EDS) was conducted using a field emission Carl Zeiss Supra 40VP SEM equipped with an Oxford Xmax 80mm^2 EDS detector, operated by Zeiss SmartSEM and Oxford AzTEC software, respectively. Computer-controlled scanning electron microscopy (CCSEM) analysis with EDS was conducted on an ASPEX PSEM, equipped with a FEI OmegaMax EDS detector and Perception feature software. No special operating conditions were necessary for SEM-EDS analysis due to small, uniform particles and the use of electrically conductive planchets.

A NIST-created software, Graf Jupiter 2016-12-20, was utilized to review and process the CCSEM raw data to remediate any potential errors (e.g., overlapping particles, contrast artifacts, sizing, and classification). For each sample, CCSEM analysis was carried out for 5,000 particulates classified as uranium-bearing via the Perception software, with bin sizes of 0.05 µm used to generate particle size distributions via CCSEM. Ex situ CCSEM and in situ APS particle size distributions were reconciled by applying a density correction factor to the

aerodynamic size measurement, which provided a simple estimate of the particulate material density.

Raman spectroscopy was utilized to assess material phase in both the prepared feedstock materials and the generated particulates. Micro-Raman spectra were acquired utilizing a Renishaw InVia Reflex Confocal Raman spectrometer coupled with two excitation lasers: a 100-mW diode source operating at 785 nm and a 50 mW Ar ion source operating at 514 nm. WiRE v5.1 software was used to control all components of the system. The InVia Reflex is calibrated by an automatic offset correction, based on the measured spectrum of an internal silicon reference material for each laser and grating combination. The laser intensity at the sample was controlled with neutral density filters and the selection of the microscope objective (primarily 100x). A spectral resolution of 0.3 cm^{-1} (full width at half maximum - FWHM), a lateral spatial resolution of 0.25 µm, and axial spatial resolution less than 1 µm were used. The InVia spectrometer employs automated beam steering optics, motorized components (Rayleigh slit, entrance slit, pinhole, multiple diffraction gratings, 100 cm^{-1} Raman edge filters, plasma line rejection filters), and dual UV-enhanced, deep depletion CCD detectors. The diffraction grating in use varied with laser selection. A 1200 grooves/mm grating was employed for all spectra acquired with the 785 nm laser while an 1800 grooves/mm grating was employed for all spectra acquired with the 514 nm laser. All Raman spectra were acquired using a 1-inch UV-enhanced deep depleted CCD detector, with six acquisitions of 60 seconds each. Power flux studies were initially performed on select particles to observe the effects of laser power on sample oxidation. Two particles were measured with 0.1, 0.25, 0.5, 1, 2.5 and 5% power, respectively. Based on this study, a laser power of 0.5% was selected to minimize oxidation. The spectra were processed using Origin 2021b software, with a smoothing filter and adjacent averaging with a 5-point window.

Thorium and uranium isotope ratios of particles were obtained using a Cameca IMS-1280 large geometry (LG) SIMS. Isotope signals were measured using a multi-collector array consisting of five electron multipliers, which counted signals from ^{232}Th, ^{235}U, ^{236}U, ^{238}U and $^{238}U^{1}H$ simultaneously. Instrument parameters included a field aperture setting of 6000 µm, an entrance slit width of 122 µm, a contrast aperture setting of 400 µm and an energy slit width of 50 µm. The operating mass resolution**,** Δm/m, where Δm is the peak width at 10% of the peak height**,** was ~1800. All other secondary ion optics and ion detector parameters were optimized to obtain quality analytical results. The primary ion beam current was adjusted to produce a ^{238}U signal of 1e5 to 2e5 counts per second (cps).

For each respective Th/U particle sample, 10 or more high-precision LG-SIMS single particle analyses were acquired. Each analysis consisted of a 240 second dwell time, split into ten 24-second cycles. A primary beam current of 1 nA and a 10 µm raster size was utilized for all single particle measurements. Prior to analysis, each particle was pre-sputtered for 10 seconds using a 25 µm-rastered beam at the same beam current as the analysis (1 nA). Final isotope ratios for each particle were calculated using the sum of counts for each isotope. Isotope ratio uncertainties of a given single particle analysis were calculated and are represented as the two-standard error (2SE) from the analysis cycles.

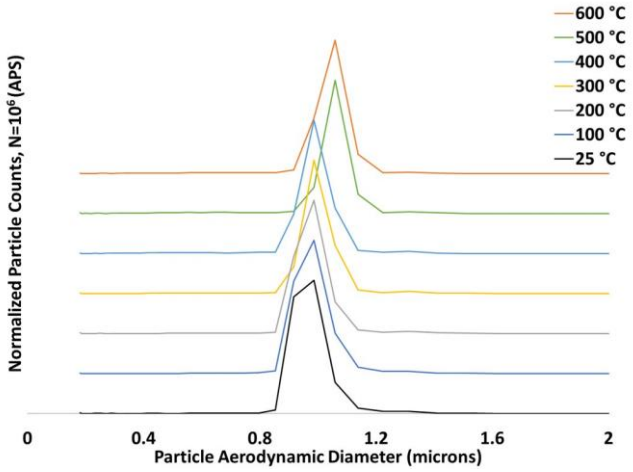

Figure 2 Aerodynamic particle size profiles of uranyl oxalate-derived particulates at temperatures ranging from 25 °C to 600 °C. APS measurements shown include a density correction ρ = 8.3 g/cm3.

LG-SIMS depth profiling measurements of single particles were also collected, using identical instrument parameters as described above. Two or more replicates per sample were run and each depth profile analysis was 2100 seconds in duration with a 1 second per cycle dwell time. Count rates were significantly diminished after approximately 1000 seconds, indicative of particle consumption (approximately 1µm of depth). As such, the provided plots of particle depth profiles show only the first 1000 seconds of data.

Isotope mapping of particle populations was also conducted for each Th/U sample using LG-SIMS. For each map, a 30 nA primary ion beam was rastered over a 250 x 250-micron area. Each mapped area was sputter cleaned (pre-sputtered) for 30 seconds prior to data acquisition, using the same primary beam conditions as the analysis. The total count time per map was 240 seconds, and isotope ratios were calculated using the total counts per isotope for each particle identified. For each sample, several map analyses (e.g. 3x3, 5x5, 5x7 arrays equating to 9, 25, and 35 locations, respectively) were collected to generate large particle datasets, and isotope ratios of identified particles were determined using Cameca's Automated Particle Measurement (APM) software.

To evaluate the isotopic homogeneity of population particle datasets, a model that predicts the scatter in data about a given isotope ratio was used, expressed as the equation (1):

$$avg.\ N/D \pm \left(avg.\ N/D \times 3.5 \times \sqrt{\frac{1}{N\ counts} + \frac{1}{D\ counts}} \right) \quad (1)$$

This predictive model is based on counting statistics, where *N* and *D* represent all possible signal combinations from the numerator and denominator of interest that correspond to a given isotope ratio (typically, the average value of a dataset).

The factor 3.5 represents a Gaussian distribution factor where 99+% of data should fall inside the upper and lower bounds of the model curves, as shown in the figures of mapped particle isotope data. If a significant number of particle data plot outside of the model bounds, this indicates that the particle population is isotopically heterogeneous for a given isotope ratio.

3. Results and Discussion

3.1 Synthesis Formulation and Optimization of Operational Parameters

Thermal inline calcination was an upgrade to the prior particle production platform and initial experiments focused on characterization of the temperature and resultant uranium product phases. Previous efforts demonstrated that particulates generated using an aerosol-based approach from uranyl oxalate solutions without the use of heat produced monodisperse particles with primarily a uranyl oxalate phase.[12] Aerodynamic particle sizing via APS was the primary diagnostic tool used, with an example of particle distribution profiles as a function of calcination temperatures shown in Fig. 2. As shown, a transition in an average equivalent circular diameter (ECD) from 1.0 to 1.1 µm with an increased inline heater temperature of 500 °C is consistent with a change in particle density, due to a thermal-induced decomposition of the uranyl-oxalate combined with the transformation to U-oxide phase. The lower temperature, less dense uranyl oxalate phase material (ρ = 3.1 g/cm^3) appears to be maintained during inline heating, up to 400 °C. This is consistent with the preservation of the modal peak position near 1.0 µm, from 25 °C to 400 °C. The shift towards a larger ECD starting at 500 °C indicates an increase in particulate density, caused by the potential onset of conversion to a uranium oxide phase (e.g., U_3O_8; ρ = 8.3 g/cm^3). It is also possible that higher particulate porosity and thermal expansion during uranyl oxalate decomposition may have led to the increased volume and size. This finding is consistent with Thermal Gravimetric Analysis (TGA) measurements of uranyl oxalate thermally induced oxidation, which show a uranyl oxalate decomposition (onset) temperature of approximately 350°C.[29]

Mixed element Th/U particulates were generated using the same particle synthesis conditions as the produced uranium oxide particles. Thorium nitrate was substituted for uranyl oxalate in the feedstock solution, at prescribed quantities, to obtain targeted thorium-to-uranium ratios ranging from 1ppm Th to samples with 10% Th/U. Aerodynamic and SEM measurements of particle size (Figure 3) show a monodisperse population, similar to that observed with regard to uranium oxide particulates prepared under similar conditions. Slight changes in particle size with changing Th compositions were observed for both aerodynamic measurements and APM-SEM. These deviations in the mean particle ECD indicate that the particulate material properties (e.g., density and phase) are measurably different at higher Th compositions.

The measured decrease in aerodynamic size, coupled to an increase in particle size (via APM-SEM) and increasing Th compositions, suggests a decrease in density, as shown in Fig. 4 and listed in Table 1. Whereas particulates up to 1% Th preserve a calculated density near that of uranium oxide (7.7 g/cm^3), the decreased density/increased size effect is most evident with the 10% Th/U particulates, where a density of 5.6 g/cm^3 was calculated (Table 1). Figure 4 demonstrates a reconciliation of density between various Th

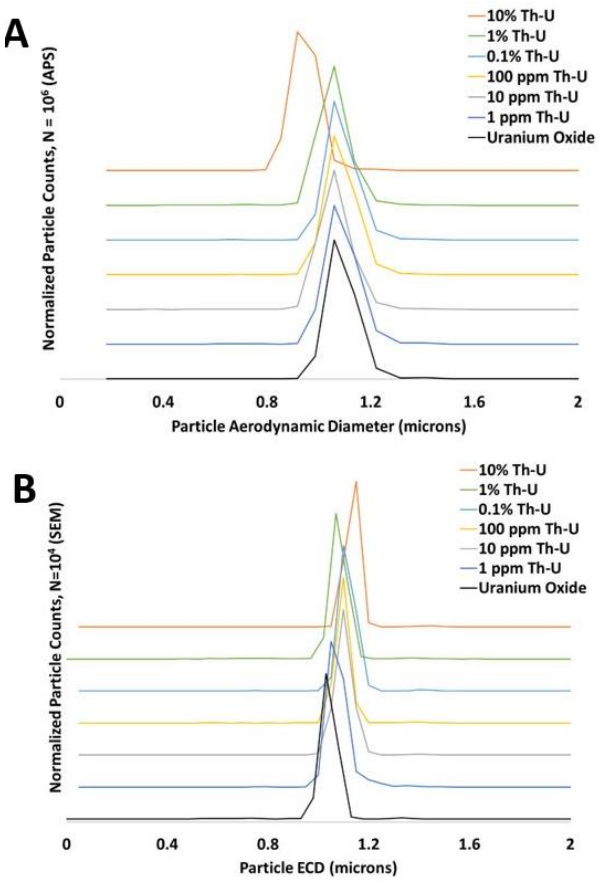

Figure 3 (A) Aerodynamic particle size profiles (density correction of ρ = 8.30 g/cm3), and (B) APM SEM size distributions of mixed uranium-thorium particulates of varying Th content.

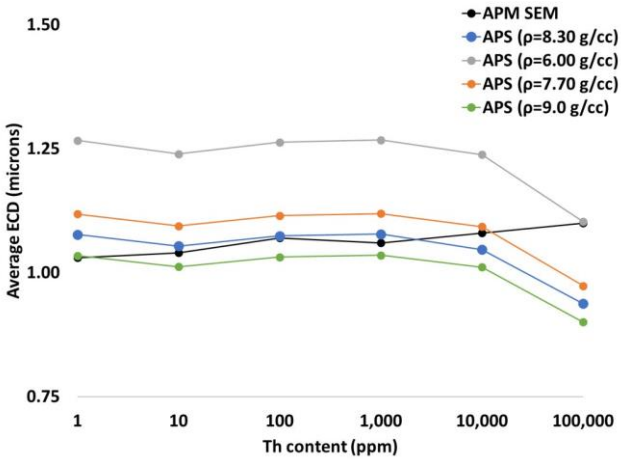

Figure 4 Comparison of average ECD from APS and APM-SEM for generated U-Th particulates with varying density corrections applied to the APS measured aerodynamic sizing. Overlay of APM-SEM and APS particle size histogram measurements with density correction are shown in profile (left) for uranium oxide only and mean histogram values for similar data per Th content (ppm).

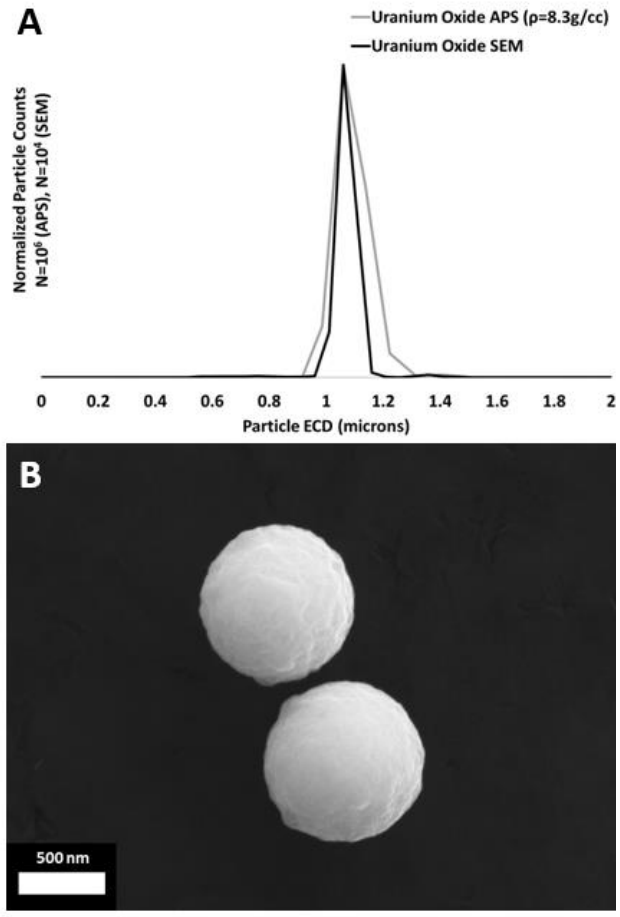

Figure 5 (A) Comparison of APS and APM SEM size distributions for uranium oxide particles generated at 600 °C, (B) exemplar uranium oxide particulates.

concentrations, wherein a convergence of APS and APM-SEM measured values predicts a density of 5.6 g/cm^3 for the 10% Th sample. The nature of the material phase for the 10% Th/U particulates is speculative, but the formation of Thoria (ThO_2)[23] and/or mixed uranium-thorium oxides is likely. For example, prior reports for the Th-U-O ternary phase system, at higher concentrations of thorium, show a mixed-phased material, such as a combination of U_3O_8 and $Th_xU_{(x-1)}O_y$, may be formed within an individual particle.[30, 31]

3.2 Characterization of product material phase and morphology

The generated uranium oxide particulates (Figure 5) display a mean particle size near 1 µm, with a monodisperse size distribution (a GSD of 1.08, measured by APS and CCSEM, respectively). The monodisperse particulate ECD distribution and average particle size are consistent with the THESEUS operational parameters for the starting concentration of uranyl oxalate (0.844 mg/mL) and droplet size FMAG setting (d = 23 µm), as well as the inline heater temperature of 600 °C. Generated particles appear spherical in morphology and lack observable surface porosity, which is consistent with calcination of the uranyl oxalate into a uranium oxide phase. Based on prior efforts utilizing uranyl oxalate to synthesize reference

Table 1 Measured aerodynamic and SEM size distribution results of the generated uranium-thorium particulates, including the calculated densities obtained by the reconciliation of APS (N = 20,000) and APM SEM (N = 5,000) sizing results

Composition	Sample ID	APS ECD (µm) (ρ=8.30 g/cm^3)	APS GSD (σG)	SEM ECD (µm)	SEM GSD (σG)	ρcalc (g/cm^3)
Uranium Oxide	20271	1.08	1.08	1.03	1.08	8.3
1 ppm Th / U	20280	1.08	1.09	1.03	1.08	8.3
10 ppm Th / U	20286	1.05	1.09	1.04	1.09	8.3
100 ppm Th / U	20292	1.07	1.10	1.07	1.12	7.7
0.1% Th / U	20298	1.08	1.08	1.06	1.08	7.7
1% Th / U	20304	1.05	1.10	1.08	1.07	7.7
10% Th / U	20316	0.94	1.10	1.10	1.08	5.6

particulate materials in the absence of inline thermal calcination, the uranyl oxalate to uranium oxide transformation likely involves multiple phases undergoing oxidation simultaneously. Similar calcination operations for particle production yielded a combination of uranyl oxalate and hydroxide, studtite, and metastudtite phases, as characterized by XRD.[12] All these phases may be present within particles post-FMAG generation and prior to calcination but no attempt was made to perform an in situ phase characterization. However, regardless of the chemical oxidation pathway, reconciliation of APS and CCSEM derived particle size distributions predict a density of 8.3 g/cm^3, which is consistent with fully dense U_3O_8 particles. These measurements are supported by single particle Raman spectroscopy measurements (see Fig. 6 wherein the spectra confirm the presence of the U_3O_8 phase.

Raman spectra were collected from samples with no Th (U_3O_8), 1% Th, and 10% Th, with representative spectra shown in Fig. 6. The uranium oxide particulate spectra and the 1% Th/U spectra are very similar and match previously reported U_3O_8 Raman spectral peak locations[32-37], as shown in Table 2.

Table 2 Summary of Raman spectra obtained for representative U/Th containing uranium oxide particles along with previously measured U3O8 measured spectra.

Raman band positions (cm^{-1})			
Reference U_3O_8	**U_3O_8**	**1% Th**	**10% Th**
137	133	131	131
236	240	238	242
342	378	374	-
408	427	425	420
480	459	451	-
738	727	731	737
811	823	821	821

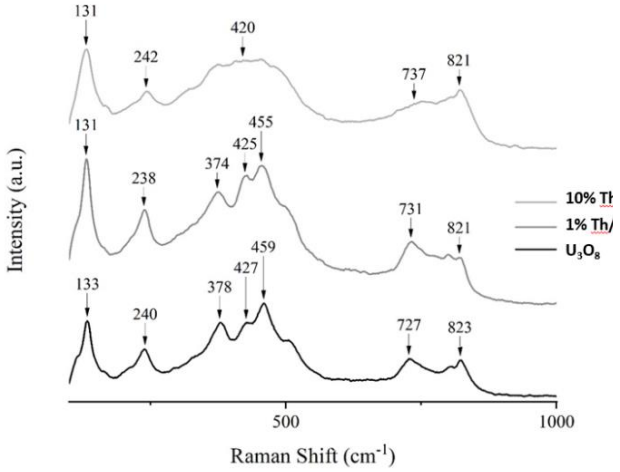

Figure 6 Representative Raman spectra (excitation laser λ = 514 nm) of representative U/Th containing uranium oxide particles synthesized with 600 °C calcination temperatures with varying Th concentrations

In contrast, as Th content increases to 10%, spectral changes become evident, with bands showing a marked broadening and a loss of relative intensity. In particular, the three Raman bands within the region of 370-460 cm^{-1} appear as one broad band centred at 420 cm^{-1}. This may be related to a reduction in uranium oxide crystalline character. Another explanation for the Raman peak broadening is a loss in crystallite size[23], which correlates to the increased surface roughness observed for the 10% Th particles over the 1% Th particles (Fig. 7). Previous studies have reported that thoria (ThO_2) exhibits a broad Raman peak at approximately 467 cm^{-1}, and that with increasing UO_2 concentration, this band will blue shift to ~450 cm^{-1}.[38-40] The broadened spectral pattern near the 420 cm^{-1} region may also occur due to overlapping uranium and thorium oxide Raman bands, and would be consistent with the mixed oxide phases determined by APS and APM SEM measurements.

An SEM comparison of the uranium oxide and Th/U particulate morphologies suggests little variation in the particle formation process (Fig. 7). The generated particles display spherical morphologies, with particle sizes near 1 µm. This is consistent with prior studies by this group regarding aerosol-based, uranium-bearing particle production, where dense uranyl oxalate spheres were formed. Energy dispersive spectroscopy (EDS) was used to qualitatively confirm the presence of Th within individual particles. However, robust quantitative analysis is not possible with current SEM/EDS instrumentation due to the limited sample volume of individual particles. However, the approximate mass per 1µm particle is likely in the range of 1-5 pg, based on U_3O_8 particles produced using a similar approach, see Richter, et al.[11]

The relative agreement in particle size and morphology (via APS and SEM measurements), within a particle population and between individual particles of varying Th compositions, suggests that the generated mixed Th/U particulates are suitable for use as particulate reference materials. While SEM and aerodynamic techniques provide a valuable assessment of

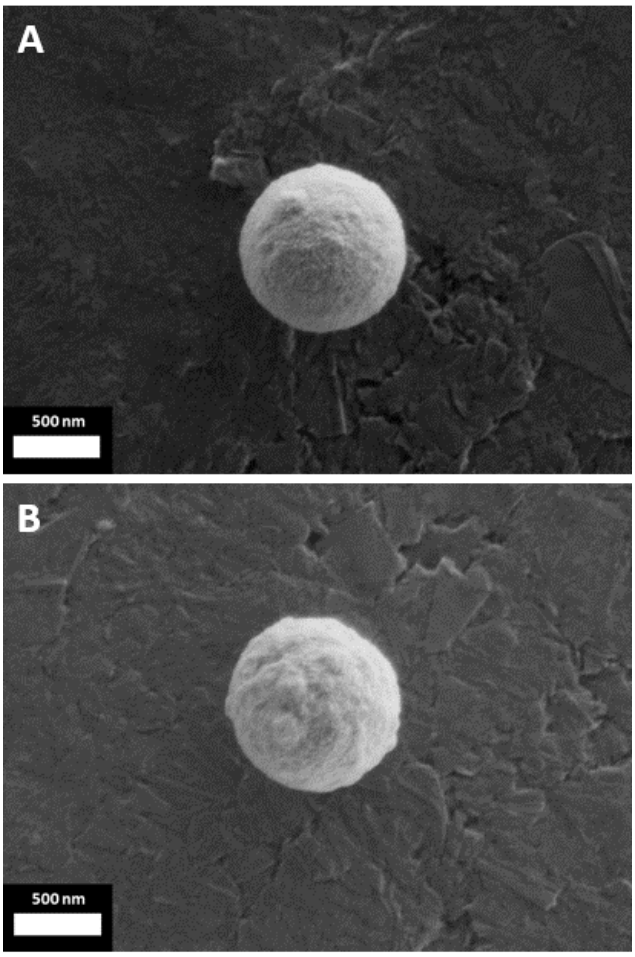

Figure 7 Exemplar particulates of (A) 1% Th/U ratio, (B) 10% Th/U ratio

inter-particle uniformity in terms of size, secondary ion mass spectrometry (SIMS) was used to provide an assessment of the inter-particle elemental and isotopic homogeneity.

Particle Characterization by SIMS

Single particle analysis results. Single particle LG-SIMS data generally display a high degree of interparticle uniformity in their $^{232}Th/^{238}U$ ratios, as a function of their total ^{238}U counts (Figure). For all single particle analysis data (N=10 per sample), the averages and expanded standard deviations (2SD) are provided in Table 3. The average and 2SD uncertainties are also shown as solid blue and dashed horizontal lines, respectively, in Figure , with the counting statistics-based homogeneity models (Eq. 1) shown as the solid red curves. Except for the 10% Th/U sample, all sample 2SD values are similar to, or better than, the predictive models of expected data scatter for a homogeneous particle population (e.g., Fig. 8A). For the 10% Th/U sample, the absolute data scatter exceeds the model of expected scatter, although the large individual particle data uncertainties put them in agreement with the model (Fig. 8C). This additional scatter in 10% Th/U may be attributed to: (1) a significant change in the $^{232}Th/^{238}U$ ratio as the LG-SIMS primary ion beam profiles through the particles (this is discussed further in the particle depth profiling results below); (2) slight differences in

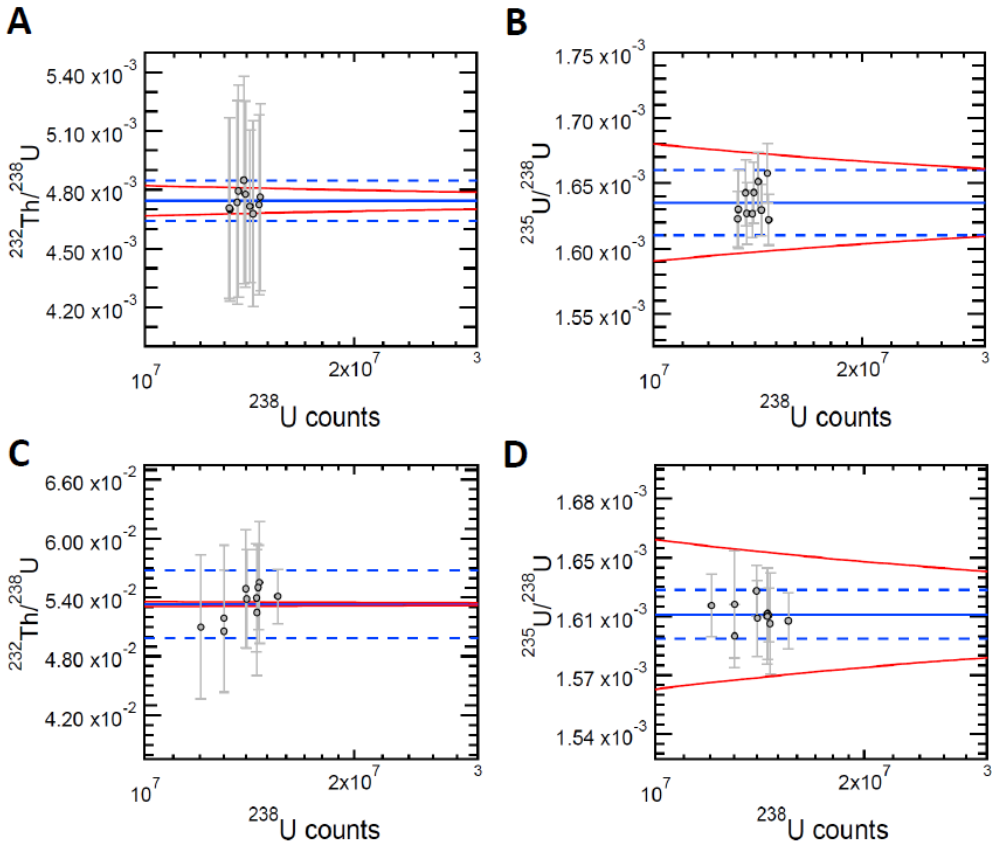

Figure 8 LG-SIMS measurements (N=10) of single particle isotope data for (A) 1% Th/U 232Th/238U, (B) 1% Th/U 235U/238U, (C) 10% Th/U 232Th/238U, (D) 10% Th/U 235U/238U.

primary beam exposure for each particle analysed, namely variations in the amount of time necessary for instrument tuning and alignment prior to each analysis; and (3) a larger extent of Th to U compositional particle-to-particle variability, which was not observed with the other samples.

For the uranium intra-element ratio, $^{235}U/^{238}U$, consistent data were obtained across the entire sample set. As shown in Figs. 8B and 8D, all data plot within the model bounds, even for the 10% Th sample (Fig. 8D), confirming intra-element isotope homogeneity. This consistency in uranium isotope ratio data was also observed with the single particle depth profiles and the isotope maps, as discussed later.

Regarding the inter-element Th/U data, a comparison of average sample Th/U ratios from single particle SIMS data versus the nominal Th/U ratio for each particle population (see Fig. 9), produces in a well-constrained linear regression with an R-squared value approaching unity. The slope of this regression, y = 0.5327x, is effectively the LG-SIMS Th/U relative sensitivity factor (RSF), defined as the ratio of the measured Th/U ratio to the known Th/U ratio of a sample. The linear correlation indicates that the LG-SIMS RSF is constant regardless of the actual Th/U ratio (or % Th composition) of samples. The regression R-squared statistic of 0.99985 suggests that the targeted Th/U ratios of each sample during production are accurate (including the 10% Th/U sample, despite a greater extent of variability between particles). Notably, all single particle measurements were analysed using identical instrument parameters, which is critical for making proper sample-to-sample RSF comparisons. The $^{232}Th/^{238}U$ based RSF determined here (0.5327) does differ slightly from the reported $^{230}Th/^{234}U$ ratio determined for uranium particle chronometry measurements, where a RSF of 0.673 with a relative standard deviation of approximately 3.6% is reported by Szakal, et. al.[18] This RSF difference between the chronometry publication and the value presented here is

Table 3 Summary of SIMS particle analysis results for Th containing uranium oxide particles. Inter-element 232Th/238U and intra-element 235U/238U ratios are provided for single particle measurements (Single P) and isotopic mapping (APM). The number of single particles measured per sample was 10 (N=10). The number of particles measured by APM ranged from 45 to 268, a dependence on particle loading and the respective number of locations analyzed per sample.

Nominal Th Composition	Single P $^{232}Th/^{238}U$	Uncert. (2SD)	APM $^{232}Th/^{238}U$	Single P $^{235}U/^{238}U$	Uncert. (2SD)	APM $^{235}U/^{238}U$
U_3O_8	6.40E-05	6.88E-06	n/a	1.65E-03	2.37E-05	1.70E-03
1 ppm	3.48E-05	2.18E-06	2.70E-05	1.65E-03	1.74E-05	1.73E-03
10 ppm	3.35E-05	6.61E-06	2.34E-05	1.64E-03	2.23E-05	1.70E-03
100 ppm	8.17E-05	8.76E-06	6.25E-05	1.64E-03	1.96E-05	1.69E-03
0.1%	5.19E-04	3.43E-05	3.69E-04	1.64E-03	2.63E-05	1.71E-03
1%	4.74E-03	1.04E-04	3.75E-03	1.64E-03	2.52E-05	1.70E-03
10%	5.33E-02	3.48E-03	1.52E-02	1.61E-03	1.45E-05	1.71E-03

likely related to the different LG-SIMS operating parameters employed between the two laboratories.

The inset to Fig. 9 shows that the samples with nominal Th/U ratios of 1 ppm, 10 ppm, and 100 ppm plot slightly above the linear regression. This observed trend is likely a product of small (tens of ppm) amounts of Th present in the depleted uranium feedstock that was used in the preparation of the Th/U sample solutions. Specifically, a comparison of $^{232}Th/^{238}U$ ratios obtained from the depleted uranium feedstock (labelled DU17 in Fig. 9) to those collected from a reference material with nominally 0 ppm Th (New Brunswick National Laboratory Certified Reference Material U030) suggests that the depleted uranium feedstock contains 60 ppm Th/U (Fig. 9)Therefore, each of the Th/U samples are likely have higher ratios than their targeted values. This effect is more noticeable for samples with the lowest Th compositions, and furthermore, explains why the 1 ppm to 100 ppm Th/U samples plot slightly above the regression line shown in Fig. 9.

Particle depth profiling results. Representative depth profiles of single particles from the 1% and 10% Th/U samples are shown in Figure 10. Note that two or more individual particle profiles were acquired from the onset of sputtering to particle consumption, per sample, and replicate profiles for each were comparable. For each plot shown the $^{232}Th/^{238}U$ ratio and ^{232}Th intensity values are scaled for visual purposes, effectively to demonstrate direct comparison to the $^{235}U/^{238}U$ ratio and ^{238}U signal profiles. The key finding from these results is that there is a difference in the $^{232}Th/^{238}U$ profiling behaviour of the 10% Th/U sample when compared to all other Th/U samples. There are also inter-element profiling differences that lead to the change in the Th/U ratio over time. More specifically, looking at the 10% Th/U sample profile plot, there is a sharp increase in the $^{232}Th/^{238}U$ ratio over the first 120 seconds of the profile, followed by a gradual decrease in the ratio from 120 to 600 seconds, then another increase in the Th/U ratio from 600 to 800 seconds, and then finally a relatively constant ratio from about 800 seconds onward is observed. This observation is in contrast to the other Th/U samples investigated, including the 1% Th/U sample provided (see Figure 10), where there is a relatively constant $^{232}Th/^{238}U$ ratio over the first 120 seconds, followed by an increase in the ratio from approximately 120 to 200 seconds, after which the ratio is relatively constant from 200 to 1000 seconds of the analysis. This notable difference in the particle profiling behaviour of the 10% Th/U sample, relative to those of the other samples, suggests a difference in the particles' internal homogeneity. The hypothesis is that the produced particles have a Th-rich crust and a Th-deficient core.

Like the single particle results, the intra-element ($^{235}U/^{238}U$) ratio did not change as a product of depth profiling (or sputtering time). As shown in Fig. 10A and 10B, the $^{235}U/^{238}U$ ratio was constant throughout the analysis duration, which is clearly different than the depth profiling behaviours of $^{232}Th/^{238}U$.

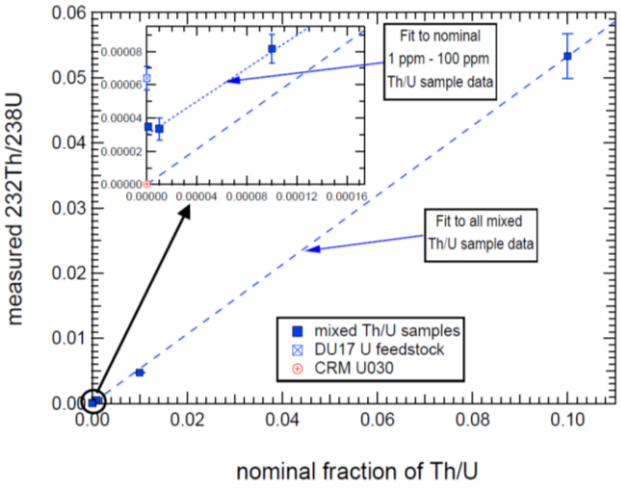

Figure 9 Correlation plot of 232Th/238U ratios measured by LG-SIMS versus the nominal Th/U ratio of the generated particles. The data used to produce this plot are provided in Table 3.

The particle depth profiles demonstrate the reason why the acquired $^{232}Th/^{238}U$ ratios of the 10% Th/U particles were not as consistent as the other Th/U samples, during single particle and isotope map analyses. The relative change in the $^{232}Th/^{238}U$ ratio observed in the 10% Th/U depth profile is significantly greater than those observed in the profiles from the other samples. At least in part, this explains why there is more particle-to-particle $^{232}Th/^{238}U$ variability for the

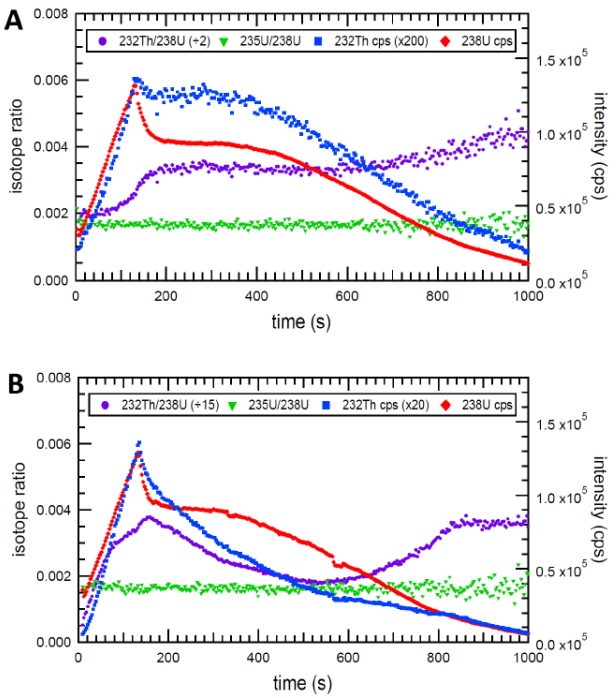

Figure 10 SIMS single particle depth profiles of a (A) 1% Th/U particle, and (B) 10% Th/U particle. The particles were fully consumed during the depth profile analyses, the approximate depth scale to reach full particle consumption was 1µm.

10% Th/U sample. Specifically, a large change in the profiling behaviour over time may result in more scatter in data if each single

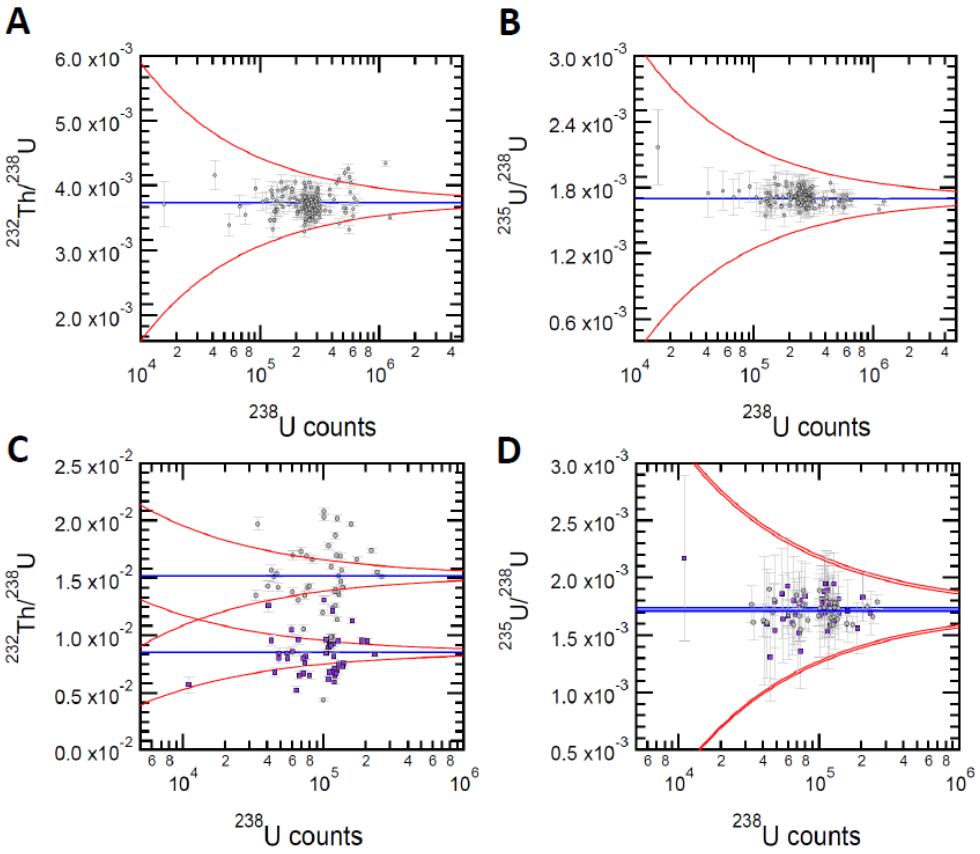

Figure 11 LG-SIMS measurements of APM isotope data mapped for (A) 1% Th/U 232Th/238U, (B) 1% Th/U 235U/238U (N=136), APM isotope data mapped for (C) 10% Th/U 232Th/238U, (D) 10% Th/U 235U/238U (N=45).

particle analysis is not started at exactly the same point along the profile. This can easily happen due to the differences in time it takes to tune and align the instrument prior to each single particle measurement. The extent of this effect is relatively muted for materials with ^{232}Th/^{238}U profiles that are more constant over time (< 10% Th). The variability in the ^{232}Th/^{238}U ratio when profiling into/through a particle reflects a level of heterogeneity within each individual particle. However, and with the exception of the 10% Th/U sample, the samples show uniformity in measured ^{232}Th/^{238}U values among the particles for a given sample, as variabilities about the average values are small. With respect to the 10% Th/U sample, the larger variability of the single particle data (Fig. 10C) and the observed heterogeneity is most likely due to the particle profiling behaviour (Fig. 10B).

Particle mapping results. LG-SIMS isotopic mapping analyses of the Th/U particle samples resulted in a range of total identified particles from 45 to 268, per sample. The variation in the number of particles found per sample was a product of particle loading (sample prep) and the number of locations (or fields of view, FOVs) measured. The 10% Th sample had the lowest number of detected particles, in part due to the repeated measurement approach discussed below. Associated mapping results are provided in Table 3 and shown in Fig. 11. The mapping results display homogeneous ^{232}Th/^{238}U ratios for each Th/U composition (e.g. Fig. 11), with the exception of the 10% Th/U sample (e.g. Fig. 11C). Specifically, for each sample, few (if any) particles plot outside the counting statistics-based model (Eq. 1; solid curved lines) about the average of the datasets (solid horizontal lines). In contrast, the 10% Th/U sample data display significant scatter outside the model bounds (see Fig. 11C). This scatter may be partially related to the large change in the ^{232}Th/^{238}U ratios of the 10% Th/U sample particles as they are being profiled/sputtered (e.g., Fig. 10B).

No data scatter was observed for the ^{235}U/^{238}U isotope maps (Figs. 11B and 11D), and collectively the samples demonstrate a similar degree of intra-element homogeneity as that observed with uranium certified reference materials, such as CRM U030.

To further demonstrate effects of profiling behaviour, the same area for the 10% Th/U sample was re-analysed (re-mapped). For the re-mapped data, an increase in the average ^{232}Th/^{238}U was found when compared to the initially mapped dataset (Fig. 11C). Additional maps were performed on the same analysis region and the ^{232}Th/^{238}U ratios for the particles located matched the changing ^{232}Th/^{238}U ratios of the depth profiling curve (Fig. 10B). These observations provide additional evidence for the larger extent of inter-particle heterogeneity for the 10% Th/U sample by comparison to the other Th/U samples. It is important to note that the discrepancies between the ^{232}Th/^{238}U averages for single particle and APM mapped datasets is reflective of the specific analytical conditions for

each type of analysis. Due to the differences in the analytical conditions, the particles are being sputtered at different rates (30 nA primary beam current, 250 µm raster for mapping versus 1 nA, 10 µm for single particle measurements). This difference, coupled with the observation that the $^{232}Th/^{238}U$ ratios change as they are profiled, shows that the LG-SIMS Th/U relative sensitivity factor (RSF) is dependent on the instrument setup parameters and analytical conditions. However, and regardless of the instrument setup conditions, if the same analytical conditions are applied (or are constant), meaningful comparisons can be made from sample to sample.

Internal Homogeneity of Sample Particles

The behaviour of the generated Th/U particle samples by LG-SIMS isotopic mapping, single particle, and depth profiling measurements, correlates well with SEM and aerodynamic size measurements, suggesting a change in the internal particle homogeneity with increasing Th content. The hypothesized Th-rich crust enveloping a Th-deficient core is believed to be produced during the particle formation process. The outer crust of the particle is formed by the effloresce of the dissolved uranium and thorium species as water is removed from the droplet during drying. The enhanced Th-content in this outer shell may be driven by the solubility limit of Th in the uranium oxide solution, along with factors related to the rapid kinetics of the drying and sintering process. The residual Th and U forms the core of the particle, where a Th-deficient phase is formed due to the depletion of the Th in solution. The observed differences in LG-SIMS depth profiling for the Th/U composition studied suggests that the threshold for the emergence of this core-shell structure exists at higher percentages of Th, and this study indicates that the threshold is somewhere between 1% and 10% Th/U. Additional investigations of the particles' internal homogeneity, using techniques such as atom probe tomography, may be required to further elucidate the effects of Th incorporation in the particle formation process.

Conclusions

This work presents a novel systematic study of Th/U micro particulates produced for nuclear reference material applications. In addition, the data supports a demonstration of sustained aerosol-based generation capability (THESEUS) for mixed-element particulate reference materials. The inter-particle size uniformity, as well as elemental and isotopic homogeneity, for particles of uranium oxide incorporated with up to 10% Th was confirmed by microanalytical techniques including scanning electron microscopy (SEM) and secondary ion mass spectrometry (SIMS). The developed aerosol-based technique, and the THESEUS production platform demonstrated in this work, are anticipated to be used in next generation particulate reference materials, in support of international nuclear safeguards. Future work will further develop the THESEUS production platform, and associated production techniques, to address current and future challenges in the field of nuclear safeguards, such as the need for mixed plutonium-uranium (Pu/U) particulate reference materials.

Conflicts of interest

The authors declare that they have no known competing financial interests or personal relationships that could have appeared to influence the work reported in this paper.

Acknowledgements

The authors wish to thank the team at the IAEA Safeguards Analytical Laboratory, and Todd Williamson from the US National Institute of Science and Technology for their expert advice and critical feedback throughout this work. This work was produced by Savannah River National Laboratory (Battelle Savannah River Alliance, LLC) and by Los Alamos National Laboratory (Triad National Security, LLC) under Contracts No. 89303321CEM000080 and 89233218CNA000001, respectively, with the U.S. Department of Energy. This work was sponsored by the National Nuclear Security Administration of the Department of Energy, Office of International Nuclear Safeguards – Safeguards Technology Development program. Publisher acknowledges the U.S. Government license to provide public access under the DOE Public Access Plan (http://energy.gov/downloads/doe-public-access-plan).

Notes and references

1. P. Doherty, A. Zoigner, K. Sirisena and E. Kuhn, *NWAL Support to IAEA Safeguards Analysis*, Report SM-367, International Atomic Energy Agency (IAEA), 2000.
2. S. Neumeier, M. Klinkenberg, P. Kegler, D. Bosbach, I. Niemeyer, R. Middendorp, C. Venchiarutti, J. Truyens, S. Richter, Y. Aregbe, L. Sangely, N. Dzigal, Z. Macsik, G. Stadelmann, S. Konegger-Kappel, T. Tanpraphan and S. Vogt, *Establishing Production and Provision of Microparticle Reference Materials for Particle Analysis through Collaboration*, Report IAEA-CN-267, International Atomic Energy Agency (IAEA), 2019.
3. R. Middendorp, M. Klinkenberg and M. Dürr, *Journal of Radioanalytical and Nuclear Chemistry*, 2018, **318**, 907-914.
4. S. Neumeier, R. Middendorp, A. Knott, M. Dürr, M. Klinkenberg, F. Pointurier, D. F. Sanchez, V.-A. Samson, D. Grolimund, I. Niemeyer and D. Bosbach, *MRS Advances*, 2018, **3**, 1005-1012.
5. IAEA, *Research and Development Plan*, Report STR-385, International Atomic Energy Agency (IAEA), 2018.
6. IAEA, *Development and Implementation Support Programme for Nuclear Verification 2020-2021*, Report STR-393, International Atomic Energy Agency (IAEA), 2020.
7. T. R. Pope, B. W. Arey, M. M. Zimmer, I. DeVore, Michael, M. G. Bronikowski, W. Kuhne, A. T. Baldwin, C. Padilla Cintron, N. C. Anheier, M. G. Warner, M. Wellons and C. A. Barrett, *ESARDA Bulletin*, 2019.
8. V. Trillaud, J. Maynadié, J. Manaud, J. Hidalgo, D. Meyer, R. Podor, N. Dacheux and N. Clavier, *CrystEngComm*, 2018, **20**, 7749-7760.

9. J. Manaud, J. Maynadié, A. Mesbah, M. O. J. Y. Hunault, P. M. Martin, M. Zunino, D. Meyer, N. Dacheux and N. Clavier, *Inorganic Chemistry*, 2020, **59**, 3260-3273.
10. J. Manaud, J. Maynadié, A. Mesbah, M. O. J. Y. Hunault, P. M. Martin, M. Zunino, N. Dacheux and N. Clavier, *Inorganic Chemistry*, 2020, **59**, 14954-14966.
11. S. Richter, J. Truyens, C. Venchiarutti, Y. Aregbe, R. Middendorp, S. Neumeier, P. Kegler, M. Klinkenberg, M. Zoriy, G. Stadelmann, Z. Macsik, A. Koepf, M. Sturm, S. Konegger-Kappel, A. Venzin, L. Sangely and T. Tanpraphan, *Journal of Radioanalytical and Nuclear Chemistry*, 2022, DOI: 10.1007/s10967-022-08255-8.
12. S. M. Scott, A. T. Baldwin, M. G. Bronikowski, M. A DeVore II, L. A. Inabinet, W. W. Kuhne, B. E. Naes, R. J. Smith, E. Villa-Aleman, T. J. Tenner, K. N. Wurth, M.S Wellons, Scale-up And Production Of Uranium-bearing QC Reference Particulates By An Aerosol Synthesis Method, 2021.
13. S. K. Potts, P. Kegler, S. Hammerich, M. Klinkenberg, I. Niemeyer, D. Bosbach and S. Neumeier, *MRS Advances*, 2022, **7**, 134-139.
14. J. J. Stoffel, J. K. Briant and D. S. Simons, *Journal of the American Society for Mass Spectrometry*, 1994, **5**, 852-858.
15. J. J. Stoffel, W. C. Cannon and D. M. Robertson, *Journal of the American Society for Mass Spectrometry*, 1991, **2**, 81-84.
16. A.-L. Fauré and T. Dalger, *Analytical Chemistry*, 2017, **89**, 6663-6669.
17. D. Suzuki, R. Tomita, J. Tomita, F. Esaka, K. Yasuda and Y. Miyamoto, *Journal of Radioanalytical and Nuclear Chemistry*, 2021, **328**, 103-111.
18. C. Szakal, D. S. Simons, J. D. Fassett and A. J. Fahey, *Analyst*, 2019, **144**, 4219-4232.
19. Z. Varga, M. Wallenius, A. Nicholl, K. Mayer, I. Balan and V. Benea, *Journal of Radioanalytical and Nuclear Chemistry*, 2019, **322**, 1585-1591.
20. P. Kegler, F. Pointurier, J. Rothe, K. Dardenne, T. Vitova, A. Beck, S. Hammerich, S. Potts, A.-L. Faure, M. Klinkenberg, F. Kreft, I. Niemeyer, D. Bosbach and S. Neumeier, *MRS Advances*, 2021, **6**, 125-130.
21. T. L. Williamson, M. A. DeVore, T. J. Tenner, R. Smith, L. Inabinent, J. Mershon, J. Hiller and M. S. Wellons, *Microscopy and Microanalysis*, 2019, **25**, 1548-1549.
22. S. K. Potts, P. Kegler, G. Modolo, S. Hammerich, I. Niemeyer, D. Bosbach and S. Neumeier, *MRS Advances*, 2022, **7**, 128-133.
23. P. Asplanato, W. Zannouh, A. L. Fauré, P. H. Imbert, J. Lautru, M. Cornaton, N. Dacheux, F. Pointurier and N. Clavier, *Journal of Nuclear Materials*, 2023, **573**, 154142.
24. *United States Pat.,* 6964189, 2005.
25. C. Carlson, DeGange, J., Cable-Dunlap, P., & Halverson, J. , *Abstract in 2nd Joint Conference on Point Detection for Chemical and Biological Defense* 2004, 81-82.
26. J. Venzie, *eDPS Aerosol Collection*, United States, 2015.
27. J. J. Katz, G.T. Seaborg, L. R. Morss, ed., *The Chemistry of the Actinide Elements, Volume 2*, Springer Dordrecht, 1987.
28. H. Tel, M. Bülbül, M. Eral and Y. Altaş, *Journal of Nuclear Materials*, 1999, **275**, 146-150.
29. N. Thompson, M. Stennett, M. Gilbert and N. Hyatt, *Journal of Radioanalytical and Nuclear Chemistry*, 2021, **327**.
30. A. Bergeron, D. Manara, O. Beneš, R. Eloirdi, M. H. A. Piro and E. C. Corcoran, *Journal of Nuclear Materials*, 2018, **512**, 324-348.
31. R. Paul and C. Keller, *Journal of Nuclear Materials*, 1971, **41**, 133-142.
32. G. C. Allen, I. S. Butler and T. Nguyen Anh, *Journal of Nuclear Materials*, 1987, **144**, 17-19.
33. I. S. Butler, G. C. Allen and N. A. Tuan, *Appl. Spectrosc.*, 1988, **42**, 901-902.
34. D. M. L. Ho, A. E. Jones, J. Y. Goulermas, P. Turner, Z. Varga, L. Fongaro, T. Fanghänel and K. Mayer, *Forensic Science International*, 2015, **251**, 61-68.
35. D. Ho Mer Lin, D. Manara, P. Lindqvist-Reis, T. Fanghänel and K. Mayer, *Vibrational Spectroscopy*, 2014, **73**, 102-110.
36. M. J. Lipp, Z. Jenei, J. Park-Klepeis and W. J. Evans, *Raman Investigation of The Uranium Compounds U3O8, UF4, UH3 and UO3 under Pressure at Room Temperature*, Report LLNL-TR-522251, awrence Livermore National Laboratory (LLNL) 2011.
37. M. L. Palacios and S. H. Taylor, *Appl. Spectrosc.*, 2000, **54**, 1372-1378.
38. K. Kamali, K. Ananthasivan, T. R. Ravindran and D. S. Kumar, *Journal of Nuclear Materials*, 2017, **493**, 77-83.
39. R. Rao, R. K. Bhagat, N. P. Salke and A. Kumar, *Appl. Spectrosc.*, 2014, **68**, 44-48.
40. M. Saoudi, D. Staicu, J. Mouris, A. Bergeron, H. Hamilton, M. Naji, D. Freis and M. Cologna, *Journal of Nuclear Materials*, 2018, **500**, 381-388.